Full Paper

Propellants, Explosives, Pyrotechnics

DOI: 10.1002/prep.201900200

Study of the Impact Energy Release Characteristics of Fine-Grained Fe–Al Energetic Jets

Qiang Li*[a] and Ye Du[a]

Abstract: Fine-grained Fe–Al energetic materials have high reaction enthalpies, and the release energy of the iron phase and a large portion of the active aluminium phase in sintered materials enables the replacement of conventional materials in new types of weapons. To study the energy release characteristics of fine-grained Fe–Al energetic jets under impact loading, a dynamic energy acquisition system is established to quantify the energy generated by the response of fine-grained Fe–Al energetic jets to impact targets. The pressure-time curves of fine-grained Fe–Al energetic jets with different ratios under different impact conditions are obtained, and a method for calculating the pressure differential value is proposed to quantitatively determine the energy release values of fine-grained Fe–Al energetic jets. The energy release mechanism of the Fe–Al energetic jet is analysed at the micro-level by recovering the reaction products. The results show that there is an optimal Fe–Al ratio that attains the greatest energy release effect from fine-grained Fe–Al energetic jets. With increasing impact energy, the energy released by energetic jets tends to increase, and an impact energy threshold that saturates the chemical reaction of energetic materials in the jets exists. The relationship between the impact conditions and the energy release value of fine-grained Fe–Al energetic jets is established.

Keywords: Fine-grained Fe–Al · Energetic jet · Dynamic energy acquisition · Impact energy · Energy release mechanism

1 Introduction

The energy released by the active metal phase in energetic materials enables the replacement of conventional materials in new types of weapons [1–3]. Researchers have found that grain refining can greatly increase the strength, combustion enthalpy and reactivity of Fe–Al energetic materials, and it has been applied to explosives and pyrotechnics [4–6]. Fe/Al composites have high strength and are inert after sinter hardening under normal conditions. However, under a strong impact load, the impact energy drives the iron phase and a large amount of the active aluminium phase in the sintered material to react violently, releasing a large amount of energy; thus, Fe–Al energetic materials can replace conventional inert materials in weaponry, such as shaped energy jets, and efficiently damage the target.

In recent years, great progress has been made in the study of Fe–Al composite materials. Jordan et al. [7] investigated the impact equation of state for Fe–Al mixtures and used light gas gun loading and explosion loading to obtain the Hugoniot parameters of energetic materials with a pressure range from 2–23 GPa. Wang et al. [8] prepared Fe–Al micro-nano composite particles with core-shell structures and found that the thermal reactivity of Fe–Al micro-nano composite powder was significantly higher than that of raw material Al powder via DSC analysis. Wang et al. [9] studied the effect of the composition ratio on the reaction heat of Fe–Al energetic materials by means of thermal analysis and micro-characterization and selected the most active Fe–Al ratio.

Energy release characteristics of energetic materials under high impact loading have also been studied. Ye and Li [10] experimentally studied the damaging effects of energetic fragments on targets such as oil tanks. Wang et al. [11] and Luo et al. [12] studied the relationship between the pressure and reaction efficiency of energetic fragments in a confined space. With increasing fragment velocity, the pressure and reaction efficiency in a confined space are increased. Ames [13] carried out an experimental study on the impact response characteristics of energetic material specimens. In the above article, the energy release characteristics of energetic materials under impact loading are studied in the form of specimens or fragments, but few studies have focused on the application of the energetic materials of jets. After all, the formation process of the fragment and the jet as well as the mechanism of releasing the energy are completely different. Therefore, it is necessary to study the energy release characteristics of energetic materials in jet form.

In view of the shortcomings of the above research, this study designs a dynamic energy acquisition system to measure the energy release resulting from the impact of fine-grained Fe–Al energetic jets on a target plate, estab-

[a] *Q. Li, Y. Du*
College of Mechatronic Engineering
North University of China
Taiyuan 030051, P. R. China
**e-mail: liqiang1170@126.com*

lishes the relationship between the impact conditions and the energy release value, analyses the critical impact energy that induces reactions in fine-grained Fe–Al energetic jets, and reveals the energy release characteristics by which fine-grained Fe–Al energetic jets impact the target plate.

2 Experimental Section

2.1 Material Preparation

The average particle sizes of the Al and Fe powders (purchased from the Beijing Xing Rong Yuan Technology Co., Ltd.) were 3.8×10^3 nm and 3.1×10^3 nm, respectively. The Al and Fe powders were mixed and milled to the nano-level in a high-energy ball mill (QM-2, Changsha Tianchuang Instrument Factory, high aluminium ceramic balls with 1 mm and 3 mm diameters, ball to powder mass ratio of 10:1). The rotational speed was 200 r/min, and the milling time was 6 hours. The relative mass ratios of Fe to Al are 2:8, 3:7, 4:6, 5:5, 6:4, 7:3 and 8:2, respectively.

To obtain a high strength while maintaining activity, the fine-grained Fe/Al composites were prepared as follows:

(1) The mixed powders were loaded into a custom mould and sintered in a vacuum hot-pressing sintering furnace (R–C-ZKQY-07, Chenrong Electric Furnace Co., Ltd. Shanghai, China), and high-purity nitrogen was used as a protective gas.
(2) After 15 minutes, the power supply for the heater was turned on, and the water-cooling system was turned on when the temperature reached 150 °C. The heating rate was set to 1 °C/min. The sintering pressure was maintained at 10 MPa.
(3) After the temperature reached the highest sintering temperature of 550 °C, the temperature was maintained for 4 hours; then, the mould was cooled to 300 °C at a cooling rate of 30 °C/h. This temperature was maintained for 1 hour.
(4) As the temperature was gradually lowered, most of the pressure was released. After the temperature reached room temperature, the mould was removed. The preparation process for the Fe/Al composites is shown in Figure 1.

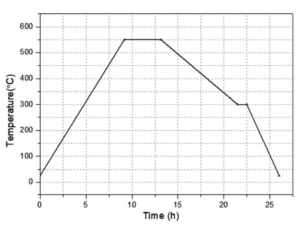

Figure 1. The Temperature Steps of a Sintering Cycle.

2.2 Test Method

The dynamic energy acquisition system consists of an Fe–Al composite shaped charge warhead (Φ40 mm), a charge ($\rho=1787$ kg/m^3, detonation velocity is 8390 m/s), a steel test vessel (Φ380 mm, with a volume of 14.67 L), a pressure testing system (BZ2202 multi-channel dynamic strain gauge, TST3125 dynamic test analyser), a pressure sensor (with a $-20\sim20$ kN pressure range, a sampling rate of 20 kHz, a sampling length of 58 s, a delay of 2 ms, and a control level of 0.15 V), a conductor, front and rear sealing plates, several Q235 steel target plates with different thicknesses, a steel protective plate, a high-speed camera and a support. The energy acquisition system is shown in Figure 2. The target plate is fixed to the steel support frame inside the test vessel by bolts, and a protective plate is placed between the test vessel and the liner to prevent detonation products and minimize the impact on the test system. To ensure that the jet enters the test vessel smoothly, a pressure relief hole of 80 mm is located in the centre of the protective plate and the front sealing plate. The axis of the liner is calibrated by a laser, and the heights of the protective plate and the front sealing plate are adjusted so that their heights are the same as that of the axis of the liner. The liner is placed on the launcher and is driven by explosive action to form a jet, which passes through the preperforated protective plate and impacts the steel baffle to produce an intense chemical reaction, releasing a large amount of heat and causing the air in the chamber to expand into an overpressure condition. The sensor at the front of the test vessel records the voltage-time signal due to the energy released by the energetic material in the jet, and the original signal is smoothed after filtering. The energy release pressure-time curve is obtained by numerical calculation.

Two series of experiments were designed to investigate the effects of the ratio of energetic materials and impact conditions on the impact energy release characteristics of fine-grained Fe–Al energetic jets, respectively.

In one set of experiments, the effect of different energetic materials ratios on the energy release was investigated. Setting the thickness of the steel diaphragm to 4 mm, the impact target plate tests were carried out for seven different Fe–Al mass ratios (2:8, 3:7, 4:6, 5:5, 6:4, 7:3, and 8:2) of energetic jets and with pure aluminium, copper and iron jets as controls, as shown from No. 1 to No. 10 in Table 1.

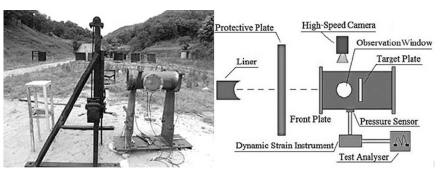

Figure 2. Energy Acquisition System.

Table 1. Experimental Parameters and Results.

No.	Mass Ratio (Fe : Al)	Target Thickness (mm)	Mass (g)	Maximum Pressure (MPa)
1	0:10	4	2.86	0.76
2	2:8	4	3.25	0.82
3	3:7	4	3.51	1.53
4	4:6	4	3.84	1.78
5	5:5	4	4.21	0.51
6	6:4	4	4.63	0.40
7	7:3	4	5.22	0.42
8	8:2	4	5.95	0.35
9	10:0	4	8.17	0.16
10	copper	4	9.39	0.25
11	4:6	2	3.84	0.97
12	4:6	2.5	3.84	1.17
13	4:6	3	3.84	1.33
14	4:6	3.5	3.84	1.52
15	4:6	4	3.84	1.77
16	4:6	4.5	3.84	1.8
17	4:6	5	3.84	1.78

In another set of experiments, the effect of the impact conditions on the energy release was investigated. Setting the mass ratio of Fe–Al to 4:6, seven kinds of steel baffles with different thicknesses (2–5 mm) were tested as impact targets, as shown from No. 11 to No. 17 in Table 1. Three experiments were carried out for each group, and the results were averaged.

2.3 Dynamic Pressure Testing Theory

Due to the limitations of the experimental conditions, it is impossible to directly measure the energy released by the fine-grained Fe–Al energetic jet under impact loading. Therefore, it is necessary to establish a correlation between the measured overpressure signal and the energy release value. First, the pressure signal is divided into two stages: the rising stage and the drop stage. The rising stage is equivalent to the sealed chamber environment. Then, the relationship between the pressure value and energy value of the sealed chamber is shown in equation (1):

$$\frac{\mathrm{d}Q}{\mathrm{d}t}=\frac{V}{\gamma-1}\frac{\partial p}{\partial t}+\frac{\gamma pV}{m(\gamma-1)}\frac{\mathrm{d}m}{\mathrm{d}t} \tag{1}$$

where Q is the internal energy increase in the closed chamber, P is the pressure in the chamber, V is the volume of the chamber, m is taken as the gas mass in the chamber, and γ is the adiabatic index, for which the chosen value is 1.4.

Ames [14] considers that the rising stage of overpressure in a chamber takes only a few milliseconds, and the *p-t* relationship is basically linear. Therefore, the existence of pressure relief holes can be neglected in the rising part of the pressure curve. If the chamber is closed and the gas mass in the chamber is constant, then process equation (1) can be simplified as follows:

$$\Delta Q_1=\frac{V}{\gamma-1}\Delta p \tag{2}$$

Equation (2) is the relationship between the peak value of the pressure in the vessel and the increase of the jet release energy during the rising stage of the pressure curve. When P reaches the peak value of the pressure, Q_1, is the maximum energy released during the rising stage of pressure. The energy released during the drop stage will be calculated below.

Ignoring the viscous and frictional heat conduction of the vessel wall, the flow of pressure relief gas can be regarded as a one-dimensional steady isentropic flow. An unconstrained pressure relief vessel is constructed. There is no heating or heat dissipation flow inside the vessel, and an ideal gas is used. The upstream and downstream states of the pressure relief port are set at the standards of 1 and 2. From the Bernoulli equation:

$$h_1+\frac{v_1^2}{2}=h_2+\frac{v_2^2}{2} \tag{3}$$

The relationship between the enthalpy h of gas in the ideal state and the parameters p and V are substituted into equation (3) as follows:

$$\frac{v_2^2}{2}=\frac{v_1^2}{2}+\frac{\gamma}{\gamma-1}(p_1V_1-p_2V_2) \tag{4}$$

For the subsonic flow of gas in the chamber, the velocity v_1 of the upstream gas flow is much lower than that of the downstream gas flow; therefore, the v_1 term in equation (4) is ignored. The amount of gas per unit time passing through the pressure relief hole of area A at velocity v_2 is shown in equation (5):

$$\frac{dm}{dt}=\frac{Av_2}{V_2} \tag{5}$$

By substituting equation (4) and the equation of state $P=\rho RT$ into equation (5), equation (6) can be obtained:

$$\mathrm{E}\frac{\mathrm{d}m}{\mathrm{d}t}=\frac{Ap_1}{T^{1/2}}\left\{\frac{2\gamma}{R(\gamma-1)}\left[\left(\frac{p_2}{p_1}\right)^{2/\gamma}-\left(\frac{p_2}{p_1}\right)^{\frac{\gamma+1}{\gamma}}\right]\right\}^{1/2} \tag{6}$$

where ρ is the gas density, R is the gas constant and T is the gas temperature. When the upstream pressure is equal to or greater than the critical pressure, $v_2=\mathrm{C}$, equation (6) can be written as:

$$\frac{\mathrm{d}m}{\mathrm{d}t}=\frac{Ap_1}{T^{1/2}}\left\{\frac{2\gamma}{R(\gamma-1)}\left[\left(\frac{2}{\gamma+1}\right)^{2/\gamma-1}-\left(\frac{2}{\gamma+1}\right)^{\frac{\gamma+1}{\gamma-1}}\right]\right\}^{1/2} \tag{7}$$

The pressure change rate in the vessel can be calculated according to the equation of state, assuming that the air temperature remains unchanged. Substituting $\frac{dn}{dt} = \frac{dm}{Mdt}$ into equation (7) obtains equation (8):

$$\frac{dP}{dt} = -\frac{RT}{V} \cdot \frac{Ap}{M} \sqrt{\frac{\gamma}{TR}} \left(\frac{2}{\gamma+1}\right)^{\frac{\gamma+1}{2(\gamma-1)}} \tag{8}$$

Equation (8) describes the theoretical curve of the pressure variation in vessels with pressure relief holes but does not consider the effect of a pressure source with continuous release on the pressure in the vessel. Therefore, when the energetic jet impacts the target plate, it releases energy continuously, which slows down the speed of pressure relief in the vessel. The measured pressure value on the time-pressure curve will exceed the theoretical value. By comparing the experimental pressure curve with the theoretical pressure curve, the part of the pressure of the former over the latter can be used to represent the energy release of the Fe/Al energetic jet during the pressure drop stage, as shown in Figure 3. The measured and theoretical pressures corresponding to the maximum pressure difference are substituted, respectively, using equations (1) and (8). By solving the above differential equation, the additional release potential value Q_2 in the stage of pressure relief can be obtained. The sum of the energy Q_1 generated in the overpressure rising phase and the energy release amount Q_2 in the pressure relief phase gives the total release energy Q_T generated by the chemical reaction of the energetic jet during the penetration process, as shown in Eq. (9):

$$Q_T = Q_1 + Q_2 \tag{9}$$

According to previous reports, the main mechanism of the chemical reaction of a metal under impact conditions is that the shockwave changes the internal structure and order of the material and causes a certain increase in temperature [15], resulting in a high-temperature and high-pressure environment in which a local hot spot forms and a rapid diffusion reaction occurs. The reaction principle for energetic materials such as explosives is basically the same. Therefore, the impact energy level becomes a scale for judging whether a chemical reaction can be induced in the energetic material and the degree of reflection. Walker and Wasley [16] proposed a method for calculating the shockwave energy, as shown in equation (10):

$$E = PU_P t \tag{10}$$

$$t = \min\left\{\frac{2r}{U_{S1}}, \frac{2h}{U_{S2}}\right\} \tag{11}$$

where P is the pressure of the jet impact loading, Up is the jet particle velocity, and t is the pulse loading time, as shown in equation (11), where r is the radius of the jet when impacting a semi-infinite target, such as thick concrete, and h is the thickness of a limited target, such as a thin steel target (thinner than the jet diameter).

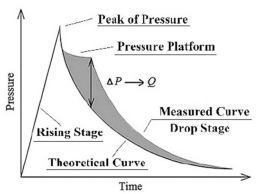

Figure 3. The Graphic of the Test Curve.

3 Results and Discussion

The energy release characteristics of energetic jets under different impact conditions are determined according to the above experimental methods and schemes. The experimental data are shown in Table 1. High-speed video of experiment No. 4 with a violent reaction is shown in Figure 4, while that of No. 6 with a slight reaction is shown in Figure 5.

Figure 4. High-Speed Video of Experiment No. 4 with a Violent Reaction.

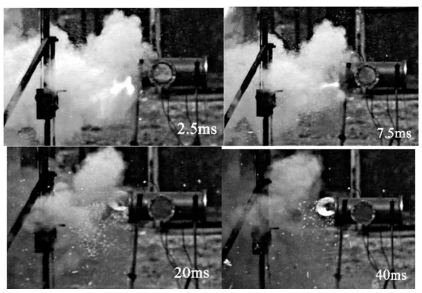

Figure 5. High-Speed Video of Experiment No. 6 with Little Reaction.

3.1 Effect of the Fe-Al Mass Ratio on the Impact Energy Release Characteristics

As shown in Figures 4 and 5, the brightness of the observation window is the highest when the mass ratio of Fe–Al is 4:6, and the sparks ejected from the pressure relief hole are the highest at this ratio, indicating that the chemical reaction of the jet after impacting the target is the most intense and the pressure formed in the chamber is the largest among the ratios.

Figure 6 shows the pressure-time curve obtained when different mass ratio jets hit the 4 mm target plate. Table 2 shows the transient release energy, pressure release energy, total release energy and specific energy calculated from the test data. Figure 7 is an analysis of the energy release characteristics of fine-grained Fe–Al energetic jets with different mass ratios.

Figures 6 and 7 show that the total release energy of the pure aluminium jet is only 30 kJ. This result is because elemental aluminium is highly agglomerated in a molten state at high temperatures [17]. After the oxidation reaction, the surface is rapidly coated with an aluminium oxide film, which blocks the internal aluminium from continuing to react with oxygen. With an increasing iron content in pure aluminium, the energy release of the fine-grained Fe–Al energetic jet is greatly improved. When the mass ratio of Fe–Al is 4:6, the peak pressure is reached, and the peak pressure, pressure release energy and the specific energy generated by the jet in the closed chamber are the highest. The specific energy value can reach 21.6 kJ/g, and the release energy effect is the best, which indicates that adding the proper amount of iron powder to the aluminium powder during the preparation of the energetic liner can greatly improve the oxidative energy release efficiency of aluminium. When the iron mass fraction reaches 50%, the energy release effect of the Fe–Al jet decreases sharply to a value even lower than that of the pure aluminium jet, indicating that the iron content in the Fe–Al composite exceeds a certain ratio, which hinders the energy release efficiency of the Fe–Al composite material. When the material

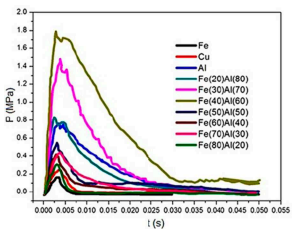

Figure 6. Comparison of Pressure-Time Curves of Fe–Al Energetic Jets with Different Mass Ratios.

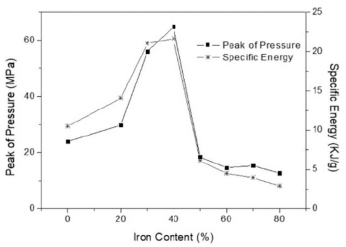

Figure 7. Analysis of the Energy Release Characteristics of Fine-Grained Fe–Al Jets with Different Mass Ratios.

Table 2. Comparison of the Impact Energy Release Values of Fine-Grained Fe–Al Energetic Jets with Different Mass Ratios.

Mass Ratio	$\bar{m}$[a] (g)	$\bar{P}_m$[b] (MPa)	Q_1[c] (KJ)	Q_2[d] (KJ)	Q_T[e] (KJ)	$Q_T/\bar{m}$ (KJ/g)
2:8 (Fe–Al)	3.25	0.82	29.8	16.0	45.8	14.09
3:7 (Fe–Al)	3.51	1.53	56.0	17.8	73.8	21.03
4:6 (Fe–Al)	3.84	1.78	64.9	18.2	83.1	21.64
5:5 (Fe–Al)	4.21	0.51	18.5	7.3	25.8	6.13
6:4 (Fe–Al)	4.63	0.40	14.6	6.2	20.8	4.49
7:3 (Fe–Al)	5.22	0.42	15.3	5.3	20.6	3.95
8:2 (Fe–Al)	5.95	0.35	12.7	4.8	17.5	2.94
Al	2.86	0.76	23.9	6.1	30.0	10.49
Cu	9.39	0.25	–	–	–	–
Fe	8.17	0.16	–	–	–	–

[a] The average mass of the liner. [b] The peak value of the overpressure. [c] The transient energy release. [d] The pressure release energy. [e] The total energy release.

is pure iron, the pressure in the vessel is the lowest among all of the studied composites.

In addition, by observing the overpressure-time curve formed by the jet with an iron mass fraction of 20%–40%, it can be found that a short overpressure plateau is formed in the pressure relief section after the overpressure peak, indicating that the fine-grained Fe–Al energetic jet under this ratio still has a period of energy release reaction in the pressure relief stage; thus, the total release energy is better than that found using other ratios.

Taking the reaction residuals of the Fe–Al mass ratios of 3:7, 4:6, and 5:5, the chemical composition analysis and comparison results are shown in Figure 8. The reaction product of the pure Al jet impinging on the 4 mm target plate was subjected to mesoscopic analysis. The results are shown in Figure 9. Comparing Figures 8 and 9, it can be seen that the compositions and contents of the recovered reaction products are approximately the same for Fe–Al mass ratios of 4:6 and 3:7, and the products are composed mainly of Al_2O_3 and Fe_3O_4, with small amounts of Fe_2O_3, aluminium and iron. No intermetallic compounds of Fe–Al were detected, indicating that the two kinds of proportioned jets experience a large amount of highly heated aluminium and that the iron oxidation reaction and aluminothermic reaction occur to a great extent during the collision of the target; in addition, because there is no Fe–Al combined reaction with a low calorific value, the energy release efficiency is high. When the mass ratio of Fe–Al is 5:5, the recovered powder contains a large amount of intermetallic compounds, such as Fe_2Al_5, $FeAl_3$ and Fe–Al, and only small amounts of metal elements and metal oxides are found, indicating that a large amount of aluminium preferentially combines with iron elements and forms an intermetallic compound with a low enthalpy. Only a small amount of aluminium participates in the oxidation reaction, which is verified from a mesoscopic perspective, revealing that the excess iron will hinder the aluminium oxidative energy release reaction. Most of the reaction products recovered after the pure aluminium jet impinges on the 4 mm target are aluminium elements that are not involved in the oxidation reaction, and only a small amount of alumina is found, indicating that the oxidation reaction rate of the aluminium jet under a high impact energy is not fast; the results obtained by microscopic analysis are consistent with the macroscopic test results in Figure 4.

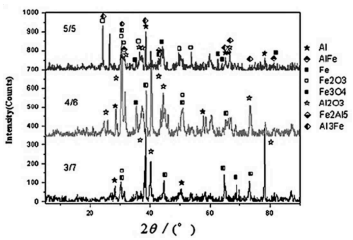

Figure 8. XRD Patterns of the Reaction Products with Fine-Grained Fe–Al Jets Impinging on 4 mm Target Plates.

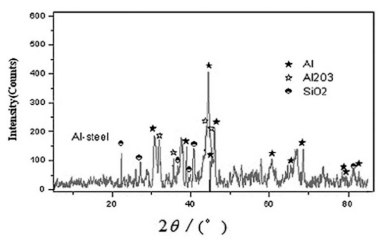

Figure 9. XRD Patterns of the Reaction Products with Pure Al Jets Impinging on 4 mm Target Plates.

3.2 Effect of the Impact Energy on the Energy Release Characteristics of Fe-Al Energetic Jets

Figure 10 shows the overpressure-time curve of energy release after data processing. Figure 11 shows the relationship between the impact energy and the energy release function. Figure 12 shows the XRD spectra of the recovered products. Table 3 compares the overpressure and energy release values of the different test schemes.

Figure 10 and Table 3 show that as the thickness of the target increases, the impact energy of the jet increases, and the pressure peak and transient energy release values of the fine-grained Fe–Al energetic jet increase. When the tar-

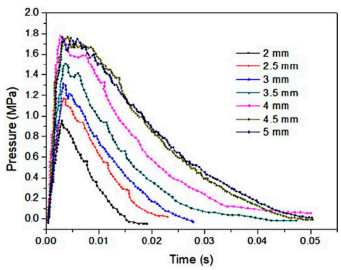

Figure 10. Comparison of the Pressure-Time Curves of Target Plates with Different Thicknesses.

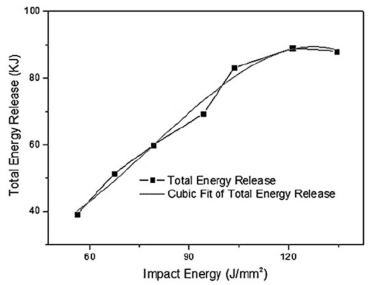

Figure 11. Fitting the Relationship Between the Impact Energy and Energy Release Function.

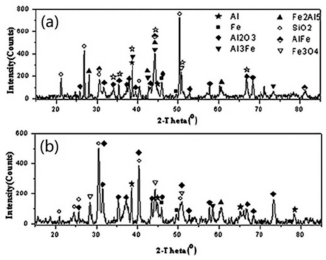

Figure 12. XRD Spectra of the Reaction Products with Different Thicknesses.

Table 3. Comparisons of Pressure and Energy Release Values of Different Testing Schemes.

Steel Plate Thickness (mm)	Impact Energy (J/mm^2)	$\overline{P}_m$ (MPa)	Q_1 (KJ)	Q_2 (KJ)	Q_T (KJ)
2	56.1	0.97	35.6	3.5	39.1
2.5	67.3	1.17	42.9	8.4	51.3
3	79.1	1.33	48.8	11.1	59.9
3.5	94.2	1.52	55.7	13.6	69.3
4	103.5	1.77	64.9	18.2	83.1
4.5	121.1	1.8	66.0	23	89.0
5	134.5	1.78	65.3	22.8	88.1

get thickness is 4.5 mm and the impact energy is 121.1 J/mm^2, the total release energy of the Fe–Al energetic jet reaches a peak of 89 kJ. When the thickness of the target plate exceeds 4.5 mm, the release energy of the fine-grained Fe–Al energetic jet does not increase further, which indicates that the chemical reaction of the energetic material in the jet reaches saturation due to the existence of a shock energy threshold of 121.1 J/mm^2. According to the regular pattern shown in Figure 10, the function of the relationship of the response induced by the shock energy loading of the fine-grained Fe–Al energetic jet is fitted by $Q = 49.89 - 1.478I + 0.03I^2 - 1.29 \times 10^{-4} I^3$ (Q: total release energy; I: impact energy), as shown in Figure 11.

It can be seen from Figure 12 that in the low impact energy recovery product, the elemental aluminium content is the highest, small amounts of intermetallic compounds are found, and no substantial amount of Fe_3O_4 is formed, indicating that the aluminium oxidation reaction and the Fe–Al intercalation reaction occur mainly under low impact energy conditions. The high impact energy scheme recovers only a small amount of metal elements and metal compounds, most of which are Al_2O_3 and Fe_3O_4, indicating that a great quantity of oxidative reactions of Fe and Al and thermite reactions are induced by the high impact energy. It can be inferred that the chemical reaction took place as shown in Eq. (12), (13) and (14):

$$Al + 3/4O_2 1/2\ Al_2O_3 \tag{12}$$

$$Fe + 2/3O_2 = 1/3\ Fe_3O_4 \tag{13}$$

$$Al + 3/8\ Fe_3O_4 = 9/8Fe + 1/2Al_2O_3 \tag{14}$$

4 Conclusions

This paper primarily studies the impact energy release characteristics of fine-grained Fe–Al energetic jets by constructing a dynamic energy acquisition test system. The influence of different material ratios and impact conditions on the energy release characteristics of fine-grained Fe–Al energetic jets is obtained. The results reveal the mechanism of fine-grained Fe–Al energetic jets as they are released by impact loading. The following conclusions are drawn from the study:

(1) Under the same impact conditions, the jet with an Fe–Al mass ratio of 4:6 has the highest pressure peak of 64.9 kJ, a release pressure of 18.2 kJ and a total release energy of 83.1 kJ, which is the highest release energy among the studied ratios.
(2) The energy released by the jet composed of iron particles with a mass fraction of 30%–40% in pure aluminium reaches 21.64 kJ/g, which is twice that of the pure aluminium jet and greatly improves the oxidative energy efficiency of aluminium. When the mass fraction of iron exceeds 40%, the energy efficiency of the jet release is reduced.
(3) The reaction behaviour of the fine-grained Fe–Al energetic jet under impact conditions is related to the impact energy. The aluminium oxidation reaction and the Fe–Al intercalation reaction occur mainly under low impact energy conditions, and a great number of oxidative reactions of Fe and Al and thermite reactions are induced by the high impact energy. With increasing impact energy, the overpressure peak and energy release of fine-grained Fe–Al energetic jets increase. There is an impact energy threshold of 121.1 J/mm^2 that saturates the chemical reaction of the energetic material in the jet.

Acknowledgements

We acknowledge Yangwei Wang and the Key Laboratory of Science and Technology on Materials under Shock and Impact for the use of their electron microscopy, EDX, and X-ray diffraction equipment. We also acknowledge Professor Chunlan Jiang for her guidance in this work. This work was supported by the China North Industries Corp. [grant number 00404010302].

References

[1] E. L. Baker, A. S. Daniels, K. W. Ng, V. O. Martin, J. P. Orosz. Barnie: A Unitary Demolition Warhead, *19th International Symposium of Ballistics*, Interlaken, Switzerland, 7–11 May 2001, **2015**.

[2] X. Zhang, X. Zhao, Review on Multifunctional Energetic Structural Materials, *Chin. J. Energet. Mater.* **2009**, *17*, 731–739.
[3] F. Peng, D. Yu, S. Yang, J. Jiang, J. Lou, W. Wang, Damage Effects of Energetic Fragment Warhead, *Chin. J. Energet. Mater.* **2011**, *19*, 450–453.
[4] S. M. Umbrajkar, M. Schoenitz, E. L. Dreizin, Exothermic Reactions in Al–CuO Nanocomposites, *Thermochim. Acta* **2006**, *451*, 34–43.
[5] H.-Z. Kang, C.-T. Hu, Swelling Behavior in Reactive Sintering of Fe–Al Mixtures, *Mater. Chem. Phys.* **2004**, *88*, 264–272.
[6] S. Izadi, K. Janghorban, G. Akbari, M. Ghafari, E. Salahinejad, Effects of Boron Addition on mechanical Alloying and Ordering Behaviors of Fe–Al–(B) Alloy Powders, *J. Alloys Compd.* **2010**, *493*, 645–648.
[7] J. L. Jordan, D. Dattelbaum, L. Ferranti, G. Sutherland, M. Baer, W. Richards, S. Sheffield, R. D. Dick, N. N. Thadhani, Shock Equation of State of Single Constituent and Multi-Constituent Epoxy-Based Particulate Composites, *AIP Conf. Proc.*, Maryland, **2009**.
[8] Y. Wang, W. Jiang, X.-F. Zhang, Z.-P. Cheng, C.-W. An, X.-D. Guo, F.-S. Li, Preparation & Characterization of Composite with Micron Al Coating in Nanometer Fe Particles, *J. Funct. Mater.* **2008**, *39*, 1900–1902.
[9] X. Wang, Y. Wang, Z. Wang, C. Jiang, Q. Li, Effect of Composition and Sintering Temperature on Reaction Heat of Fe–Al Reactive Material, *Rare Met. Mater. Eng.* **2017**, *46*, 3043–3047.
[10] X. Ye, X. Li, Experimental Study on Reactive Fragments Ignited Charge Covered with a Metal Plateafter the Impact, *Journal of Projectiles, Rockets, Missiles and Guidance* **2009**, *29*, 131–134.
[11] H.-F. Wang, Y.-F. Zheng, Q.-B. Yu, Z.-W. Liu, W.-M. Yu, Experimental Research on Igniting the Aviation Kerosene by Reactive Fragment, *Acta Armamentarii* **2012**, *33*, 1148–1152.
[12] P. Luo, Z. Wang, C. Jiang, L. Mao, Q. Li, Experimental Study on Impact-Initiated Characters of W/Zr Energetic Fragments, *Mater. Des.* **2015**, *84*, 72–78.
[13] R. Ames, Energy Release Characteristics of Impact-Initiated Energetic Materials, *Mater. Res. Soc. Symp. Proc.* **2006**, *896*, 123–132.
[14] R. Ames, Vented Chamber Calorimetry for Impact-Initiated Energetic Materials, *Proceedings of the 43rd AIAA Aerospace Sciences Meeting and Exhibit*, Reno, NV, USA, **2005**, p. 10–13.
[15] X. Zhang, X. Zhao, L. Qiao, Theory Analysis on Shock-Induced Chemical Reaction of Reactive Metal, *Explos. Shock Waves* **2010**, *30*, 145–151.
[16] F. Walker, R. Wasley, Critical Energy for Shock Initiation of Heterogeneous Explosives, *Explosivstoffe* **1969**, *17*, 9.
[17] Y.-B. Liu, *The Mechanism of Formation and Penetration of Shaped Charge Particle Jets*, University of Science & Technology China, Hefei **2012**.

Manuscript received: June 18, 2019
Revised manuscript received: November 21, 2019
Version of record online: ■■, ■■■

FULL PAPER

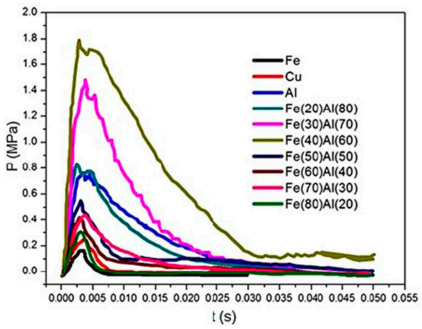

Q. Li, Y. Du*

1 – 9

Study of the Impact Energy Release Characteristics of Fine-Grained Fe–Al Energetic Jets